Organization of an Efficient Carbonic Anhydrase: Implications for the Mechanism Based on Structure−Function Studies of a T199P/C206S Mutant[†,‡]

Shenghua Huang,[§] Björn Sjöblom,[||] A. Elisabeth Sauer-Eriksson,[§] and Bengt-Harald Jonsson*[,⊥]

Department of Chemistry, Molecular Biotechnology, Linköping University, SE-581 83 Linköping, Sweden, Umeå Centre for Molecular Pathogenesis, Umeå University, SE-901 87 Umeå, Sweden, and Department of Biochemistry, Umeå University, SE-901 87 Umeå, Sweden

Received January 17, 2002; Revised Manuscript Received April 22, 2002

ABSTRACT: Substitution of Pro for Thr199 in the active site of human carbonic anhydrase II (HCA II)[1] reduces its catalytic efficiency about 3000-fold. X-ray crystallographic structures of the T199P/C206S variant have been determined in complex with the substrate bicarbonate and with the inhibitors thiocyanate and β-mercaptoethanol. The latter molecule is normally not an inhibitor of wild-type HCA II. All three ligands display novel binding interactions to the T199P/C206S mutant. The β-mercaptoethanol molecule binds in the active site area with its sulfur atom tetrahedrally coordinated to the zinc ion. Thiocyanate binds tetrahedrally coordinated to the zinc ion in T199P/C206S, in contrast to its pentacoordinated binding to the zinc ion in wild-type HCA II. Bicarbonate binds to the mutant with two of its oxygens at the positions of the zinc water (Wat263) and Wat318 in wild-type HCA II. The environment of this area is more hydrophilic than the normal bicarbonate-binding site of HCA II situated in the hydrophobic part of the cavity normally occupied by the so-called deep water (Wat338). The observation of a new binding site for bicarbonate has implications for understanding the mechanism by which the main-chain amino group of Thr199 acquired an important role for orientation of the substrate during the evolution of the enzyme.

The zinc metalloenzyme carbonic anhydrase catalyzes the interconversion of carbon dioxide and bicarbonate. The human isoenzyme carbonic anhydrase II (HCA II) is one of the fastest enzymes known with a maximal turnover rate for CO_2 hydration of 10^6 s^{-1} (*1*). The crystal structure of the 29 kD HCAII has been previously solved and refined at 1.54 Å resolution (*2*−*4*). A deep active site cavity harbors the zinc ion, which is chelated to three histidine residues and one water molecule in a tetrahedral geometry. The pK_a of the zinc-bound water molecule (the zinc water) is close to 7 (*1*). It is generally accepted that in the initial catalytic step the zinc hydroxide acts as a nucleophile attacking the carbon atom of CO_2. Numerous kinetic and inhibition studies have led to the following three-step kinetic scheme: a Zn-OH^- catalyzes the interconversion of CO_2 to HCO_3^-, leaving water as a zinc ligand (eq 1), a proton is transferred from the zinc-bound water to the imidazole ring of His64 (eq 2), and the proton is accepted by a buffer molecule from the solvent (eq 3) (*1*, *5*−*7*):

$$\mathrm{His^{64}{-}E{-}Zn{-}OH^- + CO_2 + H_2O \leftrightarrow His^{64}{-}E{-}Zn{-}HCO_3^- + H_2O \leftrightarrow His^{64}{-}E{-}Zn{-}H_2O + HCO_3^-} \quad (1)$$

$$\mathrm{His^{64}{-}E{-}Zn{-}H_2O \leftrightarrow H^+{-}His^{64}{-}E{-}Zn{-}OH^-} \quad (2)$$

$$\mathrm{H^+{-}His^{64}{-}E{-}Zn{-}OH^- + Buff \leftrightarrow His^{64}{-}E{-}Zn{-}OH^- + Buff{-}H^+} \quad (3)$$

A combination of functional and structural studies of HCA II, mutated variants thereof, and complexes with inhibitors and substrates has led to a detailed proposal for the reaction mechanism (*8*−*10*; for reviews see *11*, *12*). It has been shown that the side chains of Thr199 and Glu106, together with structurally conserved water molecules, form an extensive hydrogen bonding network important to the productive binding of the HCO_3^- substrate and for both the spatial confinement and proper orientation of the zinc-bound hydroxide for catalysis (Figure 1) (*9*, *12*, *13*). The side-chain hydroxyl group of residue T199 directs the orientation of the zinc bound hydroxide as first outlined by Merz (*14*). In addition, the main-chain amino group of Thr199 has been proposed to function both in substrate binding and in polarization of bound CO_2 (*4*, *12*). To investigate the significance of this amino group, we have constructed and characterized a variant where Thr199 is replaced by Pro, an imino acid in which the main-chain nitrogen cannot function as a hydrogen donor. The present study confirms the kinetic

[†] This work was supported by grants from the Swedish Science Councel to E.S.-E. (K5104−1098) and B.-H.J. (K5104−5999).

[‡] Coordinates for all structures described here are available at the Research Collaboratory for Structural Bioinformatics, RCSB. PDB accession codes are 1LG5, 1LG6, and 1LGD.

* To whom correspondence should be addressed. E-mail: nalle@ifm.liu.se. Phone: +46-13-288935. Fax: +46−13−122587.

[§] UCMP, Umeå University.

[||] Department of Biochemistry, Umeå University.

[⊥] Department of Chemistry, Linköping University.

[1] Abbreviations: HCA II, human carbonic anhydrase II; IPTG, isopropyl thiogalactopyranoside; PEG, poly(ethylene glycol); BME, β-mercaptoethanol; DMSO, dimethylsulphoxide; rms, root-mean-square.

10.1021/bi020053o CCC: $22.00
Published on Web 05/23/2002

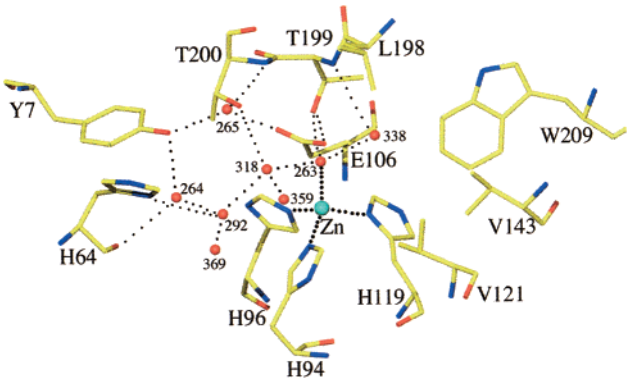

FIGURE 1: Active site of HCA II. Water molecules are drawn as red spheres, zinc ion as a larger sphere. Thick dotted lines indicate the zinc-ligand binding, and thin dotted lines indicate hydrogen bonds. Figures 1−4 were generated using O and Molray (*39*).

parameters for Pro199 (*10*) and describes its crystallographic structure in complex with HCO_3^-, β-mercaptoethanol, and thiocyanate ion, respectively. These studies provide new insights about the structural requirements for productive substrate binding and suggest possible scenarios for the evolution of the efficiency in this CO_2 hydrolase.

EXPERIMENTAL PROCEDURES

Mutagenesis. The in vitro site-directed mutagenesis was performed essentially according to the method of Kunkel (*15*) with modifications as described previously (*16*). A plasmid containing the mutation was used to transfect *Escherichia coli* BL21(DE3) (*17*). In addition to the replacement of Thr199 by Pro the studied variant also contains a C206S substitution. This replacement does not give rise to any change in specific CO_2-hydration and esterase activity compared to the wild-type HCA II (*18*) but simplifies purification and crystallization procedures. The complete coding region was verified by plasmid sequencing according to the chain termination method (*19*).

Protein Production and Purification. E. coli BL21(DE3) harboring the mutant plasmid was grown at 23 °C in 2 × Luria Broth containing 0.5 mM $ZnSO_4$ and 50 μg/mL ampicillin. Protein production was induced by adding isopropyl thiogalactopyranoside (IPTG) to a final concentration of 0.5 mM when the cell density corresponded to OD_{660} = 0.5, after which the cells were grown for another 6−12 h. The enzyme was purified in two steps using affinity chromatography (*20*), followed by ion-exchange chromatography on S−Sepharose Fast Flow (Amersham Pharmacia Biotech) as described (*21*). The purity of the enzyme was examined by SDS−PAGE.

Kinetic Measurements. Initial rates of CO_2 hydration were measured at 25 °C in an Applied Photophysics DX-17MV stopped-flow apparatus (Leatherhead, UK) by the changing pH indicator method (*22*). The buffer/indicator system, at pH 8.7, was 50 mM 1,2-dimethylimidazole/metacresol purple monitored at 578 nm. The ionic strength was kept at 0.1 M using Na_2SO_4. Rate data was fitted to the Michaelis−Menten equation using the program GraFit (Erithacus Software Ltd., UK)

Crystallization and Data Collection. Crystals were grown at 4 °C by the hanging-drop vapor diffusion method (*23*). Well solutions contained 20−22% poly(ethylene glycol) PEG 2000 or 3350, 50 mM Tris pH 7.8, and 3 mM β-mercaptoethanol (BME). Equal volumes (2 μL) of the protein solution (13 mg/mL in 25 mM Tris pH 8.0), and precipitant buffer 13% PEG 2000 or 3350, 50 mM Tris pH 7.8, and 3 mM BME were mixed and allowed to equilibrate against the resevoir solution. Crystals up to 0.3 × 0.3 × 0.2 mm^3 in size appeared after 2−3 weeks.

Table 1: Data Collection and Refinement Statistics

		T199P/BME	T199P/HCO_3^-	T199P/SCN^-
Data Collection				
space group		C2	C2	C2
cell parameters	a(Å)	72.84	73.01	66.52
	b(Å)	44.80	44.59	51.32
	c(Å)	76.46	76.64	81.00
	β(°)	92.51	92.82	107.57
no. of observations		52605	42820	22178
no. of unique reflections		22169	16497	11673
range of resolution (Å)		20−1.75	20−1.90	20−2.2
completeness (%)		93.1	88.6	91.9
R_{merge}[a]		0.066	0.089	0.113
Structure Refinement				
R factor[b]		0.205	0.188	0.197
R_{free}[c]		0.227	0.214	0.252
rmsd[d] bonds (Å)		0.010	0.011	0.017
rmsd angles (deg)		1.420	1.440	1.709
rmsd torsion angles (deg)		17207	19286	19843
no. of waters		180	166	211

[a] R_{merge} for replicate reflections, $R = \Sigma I_{hi} - \langle I_h \rangle|/\Sigma\langle I_h \rangle$; I_{hi} = intensity measured for reflection h in data set i, $\langle I_h \rangle$ = average intensity for reflection h calculated from replicate data. [b] R factor = $\Sigma||F_o| - |F_c||/\Sigma|F_o|$; F_o and F_c are the observed and calculated structure factors, respectively. [c] R_{free} is based on 10% of diffraction data randomly removed and not used in the refinement. [d] rmsd, root-mean-square deviation.

The crystals of the mutant belonged to the space group C2, in contrast to crystals of wild-type protein and previously determined mutant structures grown from ammonium sulfate. The unit cell dimensions were dependent on the molecular weight of the PEG. The cell dimensions were a = 72.8 Å, b = 44.8 Å, c = 76.5 Å, and β = 92.5° for PEG 3350 and a = 66.5 Å, b = 51.3 Å, c = 81.0 Å, and β = 107.6° for PEG 2000. Crystals from both conditions were used in the data collection.

The HCO_3^-−T199P/C206S complex was obtained by soaking the crystals stepwise, first in a solution containing 27% PEG 3350, 50 mM Tris pH 7.4, and 0.2 M NH_4HCO_3 for 30 min, followed by 0.26−0.3 M NH_4HCO_3 for 1 h, and finally 0.35 M NH_4HCO_3 for 2 h. The SCN^-−T199P/C206S complex was obtained by soaking crystals in 27% PEG 3350, 50 mM Tris pH 7.4, and 20 μM NaSCN for 2−4 h. Two crystals so treated were used for data collection.

Diffraction data sets of the BME−, HCO_3^-−, and SCN^-−T199P/C206S complexes were collected at room temperature on a DIP2030H image plate detector, using Cu−Kα radiation (λ = 1.5418 Å, double-mirror monochromatic system) generated by a Nonius FR591 rotating anode operating at 45 kV, 95 mA and bias 90. The data sets were processed and scaled using the programs DENZO and SCALEPACK (*24*), after which the intensities were converted to structure factors using the programs TRUNCATE and CAD from the CCP4 package (Collaborative Computational Project Number 4; *25*)). Details of the data collection are given in Table 1.

The structure of the BME complex was solved with the molecular replacement method using the program X-PLOR

Table 2: k_{Cat}/K_m for HCAII Mutants Relative to Wild-Type HCA II Correlated to the Presence of Deep Water

variant	K_{cat}/K_m relative to wild type (reference)	pH for measurement	pK_a of zinc water	resolution (Å)	PDB code (reference)
		Mutations with Deep Waters			
Wt HCA II[a]	100 (*5*)	8.9	6.8	1.54	2CBA (*4*)
A65F	50 (*40*)	8.0	7.2	2.00	1UGA (*41*)
A65H	100 (*40*)	8.0	7.0	2.00	1UGC (*41*)
A65L	100 (*40*)	8.0	7.1	1.90	1UGE (*41*)
A65S	100 (*40*)	8.0	6.8	2.00	1UGG (*41*)
V121A	25 (*42*)	8.5	6.8	2.40	12CA (*42*)
V143G	50 (*43*)	8.5	7.2	2.40	7CA2 (*44*)
V143H	0.9 (*43*)	8.5	6.9	2.40	8CA2 (*44*)
L198E	5.3 (*45*)	8.9	5.9	2.00	1HEB (*46*)
L198H	10 (*45*)	8.9	7.9	2.00	1HEC (*46*)
L198R	5.9 (*45*)	8.9	7.5	2.00	1HEA (*46*)
L198A	33 (*45*)	8.9	7.1	2.00	1HED (*46*)
T199A	1.0 (*8*)	8.8	8.1	1.70	1CAL (*9*)
T200S	100 (*47*)	8.5	6.9	2.10	5CA2 (*47*)
T200H	50 (*35*)	8.9	7.2	1.90	− (*13*)
P202A	100 (*48*)	9.0	na	1.70	1MUA (*48*)
		Mutations without Deep Waters			
V143F	0.046 (*43*)	8.5	7.7	2.50	6CA2 (*44*)
V143Y	0.0003 (*43*)	8.5	7.8	2.80	9CA2 (*44*)
L198F	100 (*49*)	8.8	6.8	1.95	1YDC (*50*)
T199P	0.1 (*10*)	8.9	9.2	−	−
T199P−BCT	0.03 (this work)	8.7	−	1.75	1LGD (this work)
T199C	0.1 (*51*)	9.0	na	2.10	1DCB (*52*)
T199D	0.036 (*34*)	9.0	na	2.35	1CCS (*31*)
T199E	0.036 (*34*)	9.0	na	2.20	1CCT (*31*)

[a] K_{cat}/K_m for Wt-HCAII is 1.1×10^8 $M^{-1}s^{-1}$ (*5*)

(*26*). The wild-type structure of HCA II refined at 1.54 Å resolution (PDB accession code 2CBA (*4*)) was modified (Thr199 was replaced with Gly and Cys206 was replaced with Ala) and used as the initial search model. To avoid model bias, we used the R_{free} value (*27*) from the start, with 10% of the diffraction data as the test set. The model after rotation and translation searches was subjected to rigid body minimization, resulting in R and R_{free} values of 31% and 34%, respectively, using all data between 6 and 2.3 Å resolution. The resulting $2|F_o| - |F_c|$ and $|F_o| - |F_c|$ electron density maps were inspected using the program "O" (*28*). At this point, electron densities were present that clearly identified the ring structure of Pro199 and the side chain of Ser206. These residues were subsequently built into the model. Interactive rounds of manual model building and refinement were done with X-PLOR, followed by RFMAC (*29*).

The structure of the HCO_3^- complex T199P/C206S was solved by difference Fourier techniques using the BME-complex structure as the starting model, with the BME and solvent molecules deleted. The HCO_3^- ion was rebuilt into the model on the basis of $|F_o| - |F_c|$ electron density maps and refined following the procedure described for the BME complex.

The structure of the SCN^--bound mutant structure was determined with molecular replacement methods since the crystals had a significant change in unit cell parameters (see Table 1). Again the BME complex structure without BME and solvent molecules, was used as the initial search model, and the position of the SCN^- was built in the structure based on $|F_o| - |F_c|$ electron density maps. The structure was refined as described above. Refinement statistics of the three complex structures are listed in Table 1.

RESULTS

CO_2 Hydration. Although substitution of Pro for Thr199 in HCA II drastically lowers the CO_2 hydration activity, it has been shown that the enzyme variant is still an efficient catalyst (*10*). Our results agree with these findings. The observed catalytic rates (data not shown) closely follow Michaelis−Menten patterns showing that at pH 8.7 the k_{cat}/K_m for Pro199 is approximately 3000 times lower than those for the wild-type enzyme while K_m is virtually unaffected by the mutation. The effects of other active site mutations at alkaline pH are compiled in Table 2. For example, the T199A mutation reduces the catalytic efficiency 100 times. Mutations at position 199 invariably cause an increase in the activity-linked pK_a of the $ZnOH/H_2O$ group. Thus, k_{cat}/K_m values from measurements at pH around 9 may be affected by differences in both intrinsic efficiency and pH dependence, and therefore, the pK_a values and pH of the measurement are included in Table 2.

Structure of the BME−T199P/C206S Complex. The structure of the BME complex of the T199P/C206S mutant of HCA II has been determined at 1.75 Å resolution. The final R factor and R_{free} for the mutant are 20.5% and 22.7%, respectively (Table 1). The overall structure is very similar to wild-type HCA II. Superpositioning the main-chain Cα atoms of the two structures shows a root-mean-square (rms) deviation of 0.28 Å. At the position of C206S, a new hydrogen bond is formed between the hydroxyl group of Ser-206 and the main-chain carbonyl oxygen of Val135 (the Oγ−O distance is 2.9 Å). This interaction is similar to the one in HCA I, which has a naturally occurring Ser at the position 206. Due to this interaction, the main-chain atoms of loop 127−139 are shifted about 0.8 Å toward the vicinity of the active site. With respect to native HCA II, the overall rms deviation for this loop is 0.53 Å.

Table 3: Geometry of the Zinc Ion in the Active Site of the (a) BME-, (b) HCO_3^-, and (c) SCN^--Bound Structures of the T199P/C206S Mutant of HCAII

	distance to zinc (Å)	X−Zn−94 (deg)	X−Zn−96 (deg)	X−Zn−119 (deg)	X−Zn−O2(BCT) (deg)
			(a) BME		
S2 (BME)	2.2	97.9	130.3	112.7	
Nϵ2 His-94	2.0		107.2	116.5	
Nϵ2 His-96	2.0			93.6	
Nδ1 His-119	2.1				
			(b) HCO_3^-		
O1 (BCT)	2.0	95.5	124.2	114.5	54.7
O2 (BCT)	2.7	94.4	74.4	149.8	
Nϵ2 His-94	2.0		111.0	115.4	
Nϵ2 His-96	2.0			97.4	
Nδ1 His-119	2.1				
			(c) SCN^-		
N (SCN^-)	1.9	105.2	149.1	91.6	
Nϵ2 His-94	2.1		94.1	120.1	
Nϵ2 His-96	2.1			99.5	
Nδ His-119	2.1				

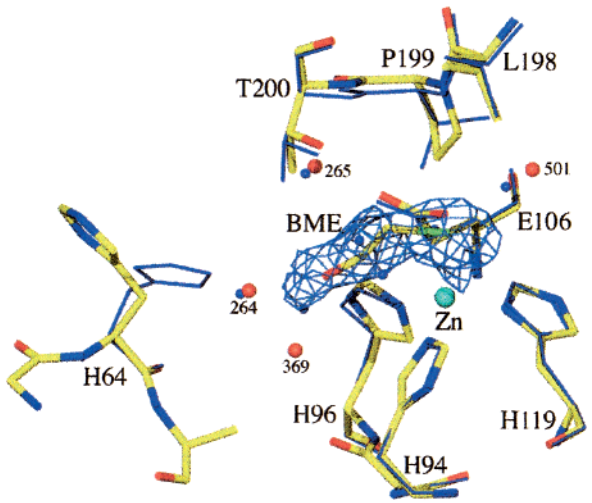

FIGURE 2: $|F_o| - |F_c|$ electron density map of the T199P/C206S mutant in complex with BME. The map shows the density over the BME molecule contoured at 3ó, where σ is the rms density throughout the unit cell. Superimposed native HCA II coordinates are shown in blue. To reduce model bias, we excluded and subjected the BME molecule to one round of refinement (REFMAC) prior to the map calculation.

The mutated region at the active site including residues 198−202 is only slightly shifted with an rms deviation of 0.09 Å. The main-chain atoms of residue Pro199 are moved away from the center of the active site with a shift of about 0.45 Å. The rms deviation for the main chain of the three zinc binding histidine ligands is, however, only 0.03 Å.

The extensive hydrogen bonding network in the active site of HCA II consisting of the Zn-bound H_2O/OH^- (Wat-263), the "deep-water" (Wat-338), and the additional active site water molecules (Wat-318, Wat-292, and Wat-359) (Figure 1) is missing in the mutated structure. An extraneous, slightly curved density appears in the vicinity of the zinc ion, as indicated in both the $2|F_o| - |F_c|$ and $|F_o| - |F_c|$ electron density maps (Figure 2). The highest peak (visible at contour levels over 5σ in $|F_o| - |F_c|$ maps) is situated 2.4 Å from the zinc ion, at one end of the density. With the composition of the crystallization medium in mind, we tried to model water molecules, BME, SO_4^{2-}, HCO_3^-, or Tris ions into this density. The density shape and the refined temperature factors only matched for a BME molecule. This is the first time a BME molecule has been reported to interact with the active site zinc of HCA II. The affinity for BME was therefore studied in an experiment to measure the inhibition of the CO_2 hydration reaction by BME at pH 7.8 (data not shown). Due to the low catalytic efficiency of this mutant, it was difficult to measure the inhibition constant with high accuracy, but the data indicate that the enzyme was 50% inhibited at 1−2 mM BME. In the complex structure, the sulfur atom of BME, together with the three ligands His94, His96, and His119, forms a distorted tetrahedral coordination geometry on the zinc ion (see Table 3). There are no hydrogen bonding partners in the vicinity of the sulfur; the distance to the Oγ1 atom of Thr200 is 4.9 Å. The BME molecule is situated near the positions of Wat-263, Wat-318, and Wat-292 in the HCA II structure (see Figure 1). Besides binding to the zinc, the sulfur atom is also in the vicinity of the Cβ and Cδ atoms of Pro199 (3.3 and 3.2 Å, respectively) and is situated 3.1 Å from the Nϵ2 atom of His94. The shift from the original zinc-bound Wat-263 in the wild-type structure is 0.8 Å. The hydroxyl group of BME displaces the original Wat-292 (a shift of 1.1 Å) and forms a hydrogen bond with Wat-369 and Wat-264 (with O−O distances of 3.0 and 3.1 Å, respectively). These in turn form two hydrogen bonds to the carbonyl oxygen of His64 and the hydroxide oxygen of Tyr7, respectively. The carbon atom C1 of BME is situated at the position of Wat-318 (shift is 0.6 Å). The temperature factor for the refined zinc ion is 16.0 Å^2, and for the BME atoms O1, C1, C2, and S2, the temperature factors are 35.0, 32.5, 30.7, and 26.0 Å^2, respectively.

Residue Glu106 maintains a position in the T199P/C206S mutant similar to that in wild-type HCA II. In agreement with the structures from the previously reported mutants Thr199Ala, Thr199Asp, and Thr199Glu, we also found the new water molecule Wat-501 hydrogen bonded to the Oϵ1 atom of Glu106 (the distance is 2.7 Å). The function of this water is most likely to compensate for the broken hydrogen bond between the Oϵ1 atom of Glu106 and the Oγ1 atom of Thr199 (*9*). His-64 has a fixed orientation, which corresponds to the "out" conformation previously found only in low pH (5.6) crystal structures of HCA II (*30*).

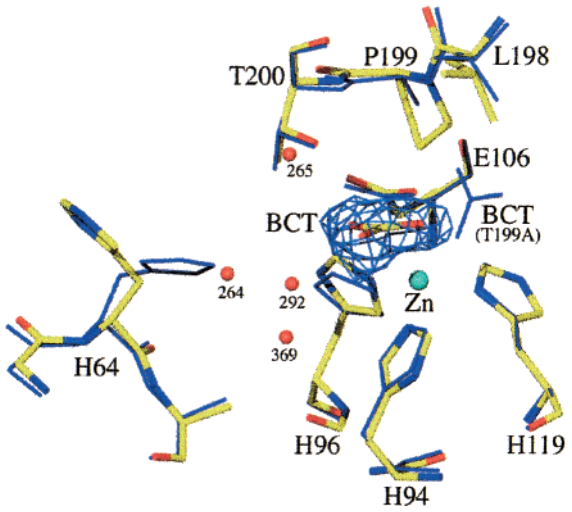

FIGURE 3: $|F_o| - |F_c|$ electron density map of the T199P/C206S mutant in complex with bicarbonate. The map shows the density over the bicarbonate molecule contoured at 3σ. Superimposed coordinates for the Thr199A−bicarbonate complex are shown in blue, and the position for bicarbonate is indicated (BCT). The map was calculated as described in Figure 2.

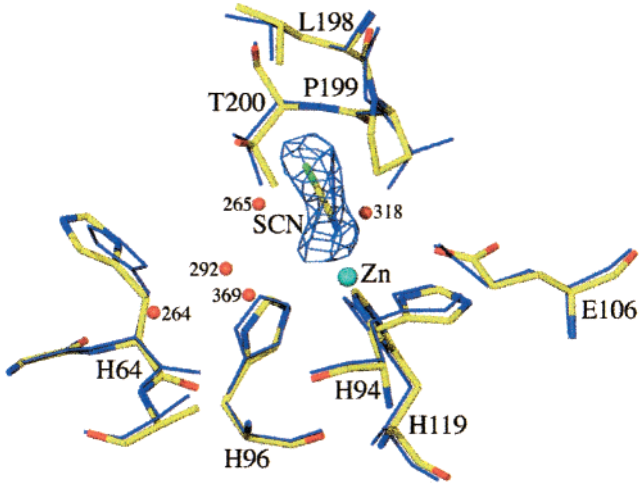

FIGURE 4: $|F_o| - |F_c|$ electron density map of the T199P/C206S mutant in complex with thiocyanate. The map shows the density over the thiocyanate molecule contoured at 3σ. Superimposed coordinates for native HCA II are shown in blue. The map was calculated as described in Figure 2.

In attempts to obtain the structure of the apo T199P/C206S mutant, crystals were soaked in inhibitor-free solutions. Unfortunately, the crystals diffracted poorly; however, adding zinc binding compounds (SCN^-, HCO_3^-, and BME) immediately improved the diffraction quality. These results agree with previous data showing that even though the active site in carbonic anhydrase is buried in a deep cavity, the zinc geometry affects the diffraction quality of the protein crystals (*9*, *31*).

Structure of the Bicarbonate-T199P/C206S Complex. The structure of the HCO_3^- complex was refined at 1.9 Å resolution with a final *R* factor and R_{free} of 18.7% and 21.0%, respectively (Table 1). The rms deviation of the Cα atoms for the complex and the native enzyme is 0.28 Å. The main-chain atoms of residue Pro199 are moved away from the center of the active site about 0.45 Å, similar to what was observed for the BME-bound complex.

At the active site, the slightly curved electron density corresponding to the BME molecule had disappeared, and instead, a triangular and near-planar shaped density appeared in the vicinity (Figure 3). This peak was interpreted as originating from a bound HCO_3^- anion since Tris buffer and sulfate ion were also modeled but did not fit the density. Zinc water (Wat-263), "deep-water" (Wat-338), and Wat-318 in the active site of wild-type HCAII are not present in the structure. The coordination geometry of the zinc ion is a distorted tetragonal pyramidal (Table 3) in which the HCO_3^- anion functions as a pseudobidentate zinc ligand. One of its oxygen atoms, O1, is located near the position of the original zinc water (Wat-263, shift 0.6 Å) at a distance of 2.1 Å from the zinc ion, 3.0 Å from the Cγ atom of Pro199, 3.1 Å from Wat-389, and 2.6 Å from a new molecule Wat-502. The second oxygen atom, O2, of the HCO_3^- ion is situated 2.7 Å from the zinc ion, 2.8 Å from Wat-292, and 3.0 Å from the Cγ2 atom of Thr200. The third oxygen atom, O3, forms hydrogen bonds with the Oγ1 atom of Thr200, Wat-292, and Wat-389 at a distance of 3.1, 2.8, and 2.6 Å, respectively. This oxygen atom is situated close to the position of Wat-318 in the wild-type structure (shift 0.6 Å). The new water molecule Wat-501 forms a hydrogen bond to the Oϵ1 of Glu106 (O−O distance 2.8 Å). The position of the HCO_3^- anion in the T199P/C206S mutant is unique. In the two previously solved HCO_3^- complex structures of Thr200His and Thr199Ala, both HCO_3^- anions are located at the position between the zinc-bound Wat-263 and the deep-water Wat-338 (*9*, *13*). The distance between the centrally positioned carbon atom of the HCO_3^- ion in the T199P/C206S complex and the same atom in the HCO_3^-−Thr200His complex is 2.7 Å. The corresponding distance between the two bicarbonate carbons in the HCO_3^-−Thr200His complex and the HCO_3^-−Thr199Ala complex is 0.4 Å. The introduced Pro at position 199 occupies part of the space for the deep water and prevents binding of HCO_3^- at this site. The temperature factor for the refined zinc ion is 10.9 Å^2, and for the HCO_3^- atoms C, O1, O2, and O3, the temperature factors are 32.2 Å^2, 29.7 Å^2, 32.9 Å^2, and 33.8 Å^2, respectively. The positions of the residues His64 and Glu106 are identical to those in the BME-bound T199P/C206S mutant.

Structure of the Thiocyanate−T199P/C206S Complex. The SCN^- complex of T199P/C206S HCA II was refined at 2.2 Å resolution with final *R* factor and R_{free} values of 19.7% and 25.2%, respectively (Table 1). The rms deviation of the Cα atoms of the wild-type protein and the SCN^--bound complex is 0.35 Å, and the rms deviation of the Cα atoms of the SCN^--bound complex and the BME-bound complex is 0.30 Å.

The difference $|F_o| - |F_c|$ electron density map revealed an elongated density at a contour level of over 6σ (Figure 4). This density is situated in the vicinity of the zinc ion and clearly shows the position of the thiocyanate ion. The ion binds in a slightly different conformation compared to its binding site in the wild-type structure (*32*). The position of its nitrogen atom is shifted 0.3 Å, and the linear SCN^- molecule is directed away from the position of Pro199, forming an angle of about 20° to its position in the wild-type structure. However, the major difference in the binding interaction in the two complexes is that the zinc-bound water (Wat-263) is displaced in the SCN^--bound T199P/C206S

structure, thus maintaining the tetrahedral geometry of the zinc ion (Figure 3). In the wild-type structure, SCN^- binds in a pentacoordinated fashion, and both Wat-263 and the nitrogen atom of SCN^- act as zinc ligands. In addition to the zinc water, the "deep-water" Wat338, Wat-359, and Wat-389 are not present in the active site of the T199P/C206S structure. The distance from the nitrogen atom of SCN^- to the zinc ion is 1.9 Å, and the distances to the Cγ and Cδ atoms of Pro199 are 3.3 and 3.4 Å, respectively. The sulfur atom of SCN^- is situated 3.2 Å from the Cδ2 atom of Leu198. The temperature factor for the refined zinc ion is 21.2 Å^2, and for the SCN^- atoms S, C, and N, the temperature factors are 27.7, 27.2, and 28.0 Å^2, respectively. Residue Glu106 remains in the same position as in the BME- and HCO_3^- -bound complexes. The water molecule Wat-501 forms a hydrogen bond to the Oϵ1 of Glu106 (O−O distance 2.9 Å). The His64 residue is oriented identical to the "out" conformation.

DISCUSSION

The X-ray crystallographic analysis of HCA II in the past has shown that the catalytic zinc ion is tetrahedrally coordinated by three histidine residues, with the fourth ligand being a water molecule or a hydroxide ion (*2*). There is an extensive hydrogen bonding network in the active site leading from the zinc ion to the bulk water (Figure 1). This network initiates from the zinc-bound OH^-/H_2O and proceeds via a hydrogen bond to the hydroxyl oxygen of Thr199, which in turn is linked to one of the carboxylate oxygens of Glu106. The other carboxylate oxygen of Glu106 is hydrogen bonded to the main-chain amino group of Arg246. Both Glu106 and Thr199 are strictly conserved in all sequenced animal carbonic anhydrases (*33*). The roles of Glu106 and Thr199 in elementary catalytic reactions have been investigated in several studies of the site-directed mutants Thr199 to Ala (*8*, *9*), Thr199 to Ser, Ala, Val, Asp, Glu, and Pro (*10*, *34*), and mutants of Glu106 to Ala, Asp, and Gln(*8*, *9*). The CO_2 hydration activity (k_{cat}/K_m) of Ala199 is 100-fold lower than that for the wild-type enzyme, while k_{cat}/K_m for Gln106 is reduced 10-fold (*8*, *9*). Merz (1990) suggested that the zinc-bound hydroxide ion, because of its specific interaction with the zinc ion and its direct hydrogen bonding to the Thr199 Oγ1 atom, is ideally positioned for a nucleophilic attack on a CO_2 molecule bound in the deep-water position (*14*). This is supported by the Glu106Gln mutation where the orientational control of the zinc hydroxide is lost because of a reversed hydrogen-bond pattern at the hydroxyl group of Thr199 (*9*). In the Thr199Ala mutant, the hydrogen bond to the zinc hydroxide is lost, altering the spatial position of the hydroxyl group. It has been estimated that the control of the orientation of the zinc-bound hydroxide contributes by a factor of 10 to the catalytic efficiency. The correct positioning of the hydroxide contributes an additional factor of 10 (*12*).

Notably, the zinc-bound hydroxide is itself also tetrahedrally coordinated to the zinc ion, the Oγ1 atom of Thr199, the deep-water (Wat-338), and the water molecule Wat-318 (Figure 5A). In addition, each of the three hydroxide ion ligands is stabilized by a second hydrogen bond: the Oγ1 atom of Thr199 is hydrogen bonded to the Oϵ1 atom of Glu106, the deep water makes a weak hydrogen bond to the backbone amino group of Thr199, and the water molecule Wat-318 is hydrogen bonded to the Oγ1 of Thr200 and Wat-292. Mutations in the active site area, including the T199P/C206S mutation, affect this delicate network of hydrogen bonds. As a result, these mutations also have distinct effects on the binding of bicarbonate as will be discussed.

The structure of the HCA II mutant Thr200His in complex with bicarbonate shows that the protonated oxygen atom in bicarbonate displaces the zinc hydroxide ion and maintains the hydrogen bond to Thr199 (*13*). Its second oxygen atom is close to the deep-water position (the shift in position is 0.7 Å), making a hydrogen bond to the main-chain amino group of Thr199 (Figure 5B). The side chain of His200 displaces the water molecule Wat-318. We propose that this structural arrangement represents the normal bicarbonate-binding mode in the high-activity carbonic anhydrases (eg., HCA I and HCA II) since the catalytic properties of this mutant lie somewhere between those of the two "natural" enzymes. k_{cat}/K_m, at high pH, for the Thr200His mutant is 6.2×10^7 $M^{-1}s^{-1}$, which is 60% of k_{cat}/K_m for HCA II (*35*).

In the mutant Thr199Ala the binding site for bicarbonate is close to that seen in the structure of Thr200His (*9*, *13*). The bicarbonate molecule binds in the position of the deep water with one of its oxygen atom hydrogen bonded to the backbone nitrogen proton of the residue 199 and with the second oxygen coordinated to the zinc ion. The only difference between the two bicarbonate complexes is that in Thr199Ala the zinc hydroxide ion is not displaced but has moved 1.6 Å in the direction of Glu106, making the zinc ion pentacoordinated rather than tetracoordinated (Figure 5C). In addition, a new water molecule is coordinated to one of the Oϵ atoms of Glu106. This water molecule fills the space created by the reduced size of Ala199 (*9*).

The structure of T199P/C206S, in complex with bicarbonate, revealed a strikingly different binding of bicarbonate. One of the bicarbonate oxygen atoms displaces the zinc hydroxide ion as seen in the Thr200His complex, but the second oxygen atom is not hydrogen bonded to the main-chain amino group of residue 199 as in the two previously described structures. Instead, the bicarbonate is bound on the opposite side of the zinc hydroxide ion at the position formerly occupied by water molecule Wat-318, thus making a hydrogen bond to Thr200. The deep water is displaced by the ring structure of the Pro199 (Figures 3 and 5D) leaving no room for bicarbonate at its usual site. The structure has new water at the same position as that found in the Thr199Ala mutant. The catalytic ability of this mutant is very much decreased, not only compared to the wild-type enzyme (k_{cat}/K_m is 2800-fold lower) but also compared to the Thr200His and Thr199Ala mutants (Table 2).

In the T199P/C206S mutant, the hydrogen bond between residue 199 and the zinc-bound hydroxide ion is removed, as is the possibility for hydrogen bonding to the backbone amino group of residue 199. Thus, the novel bicarbonate binding site does not provide a nearby hydrogen-bond acceptor that could dictate the orientation of the zinc-bound ion. This is in contrast to the wild-type enzyme in which the hydroxyl group of Thr199 forces the hydroxyl group of the bicarbonate to be the obligatory zinc ligand (*12*). The observation of a new binding site for bicarbonate in the structure of T199P/C206S implies a new binding site for CO_2 in the vicinity of what is usually the binding site for Wat-318. This site has two features in common with the normal binding site: the distance to the hydroxide ion is similar (2.8 Å compared to 2.6 Å), and there exists a hydrogen bonding

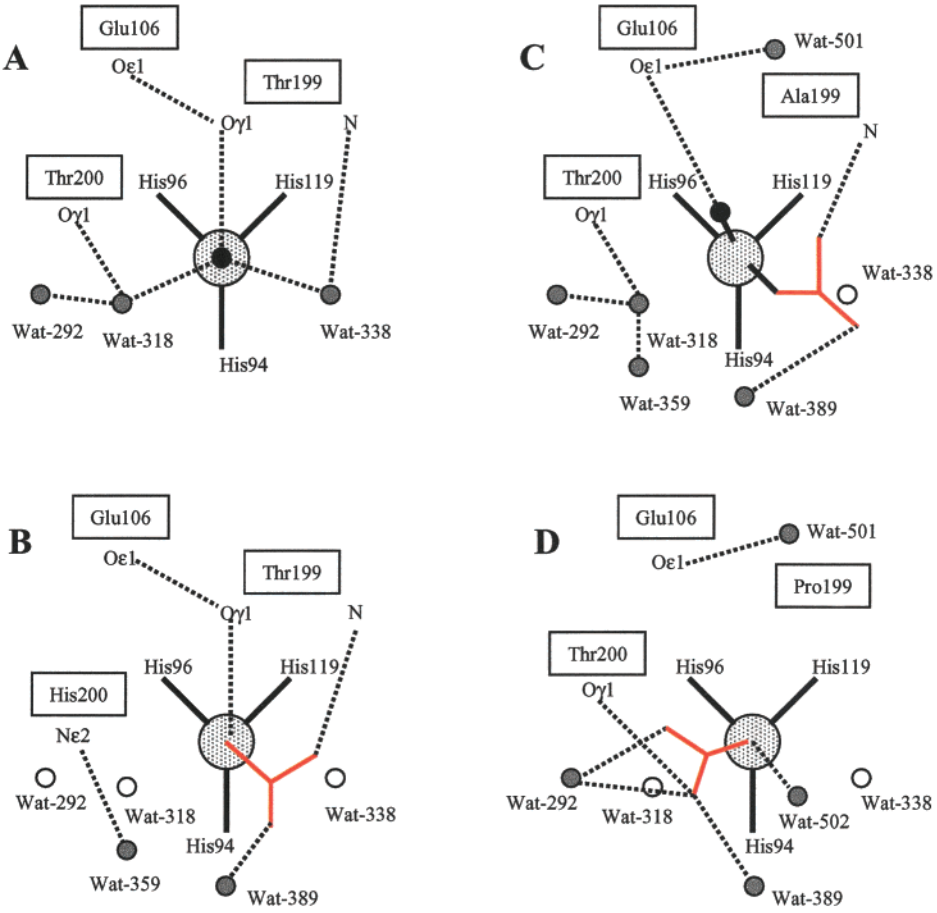

FIGURE 5: Schematic drawing of the coordination geometries in the active site of wild-type and mutant HCA II looking down the zinc-Wat263 bond. (A) The geometry in native HCA II (pdb code 2CBA). (B) The position of bicarbonate in Thr200His (pdb code 1BIC). (C) The position of bicarbonate in Thr199Ala (pdb code 1CAM). (D) The position of bicarbonate in T199P/C206S (this work). The inner-shell ligation to the zinc ion is shown in thick black lines. The large dotted gray circle and the black smaller circle represent the zinc ion and the zinc-bound water/hydroxide ion, respectively. Smaller gray circles are water molecules present in the structure. White circles are water molecules present in wild-type HCA II but missing in the complex. Bicarbonate is shown as red sticks and hydrogen bonds as dotted lines.

possibility, to the Oγ1 atom of Thr200, rather than the main-chain amino group of residue 199 in the wild-type enzyme. The major difference is that the novel CO_2 binding site has a hydrophilic environment whereas the normal site is situated in the hydrophobic pocket at the deep-water position. The new active site of the T199P/C206S mutant has a drastically decreased catalytic ability compared to that of the wild-type enzyme but can still be considered a good catalyst. The observation of that the T199P/C206S mutant, in contrast to the wild-type enzyme, is inhibited by BME indicates that the introduction of a novel ligand binding site not only leads to diminished catalytic efficiency but also results in an enzyme that is more susceptible to inhibition.

We have compared all mutant variants of HCA II available in the protein databank, excluding only variants in which one of the three histidine ligands to the zinc is mutated or structures that include bound inhibitors. The remaining structures were divided into two classes: those which maintain the deep water in their structures and those which do not. A comparison of the catalytic activities of the protein variants within and between these two classes reflects class-specific variations in their k_{cat}/K_m (Table 2). Mutants of HCA II that still possess the deep water are generally more active than mutants that do not. The maximum decrease in k_{cat}/K_m relative to the wild type for mutants maintaining the deep water (e.g., Thr199Ala) is about 100-fold, whereas mutants without the deep water (e.g., Thr199Cys) display a minimum decrease of about 1000-fold. There exist only one exception that does not follow the above-mentioned pattern. The structure of Leu198Phe does not contain the deep water but has a k_{cat}/K_m value about the same as that for the wild type. The class lacking the deep water can be further divided into two groups depending on the type of mutation. One group (Thr199Cys, Thr199Asp, and Thr199Glu) contains mutations that create a new zinc ligand that displaces the zinc hydroxide ion, and the second group contains mutations in which the deep water is displaced without disturbing the zinc ligands. The later group contains the two mutants, Val143Tyr and Val143Phe, which both are too bulky to leave any space for the deep water and will therefore not allow CO_2 to enter at its normal binding site. The CO_2 molecule has to find a new binding site where it can be subjected to a nucleophilic attack from one of the free electron pairs of the zinc hydroxide ion. The only remaining suitable position where this can occur is at the site of water molecule 318. We argue that CO_2, in complex with these two mutants, makes use of the same binding site as that in the T199P/C206S mutant. We refrain from speculating about the position of the CO_2-binding site for the mutants belonging to the first subgroup (Thr199Cys, Thr199Asp, and Thr199Glu) because replacing the zinc hydroxide with a different ligand may lead to a different mechanism.

These observations about the various effects on catalytic efficiency and substrate binding caused by mutations of residues surrounding the zinc hydroxyl group allow us to construct a model for the evolution of an efficient carbonic anhydrase. From an evolutionary point of view, the first productive feature created would most likely have been the ability of the enzyme to bind a tetrahedrally coordinated zinc ion with a water/hydroxide ion serving as its fourth ligand. At this stage, the substrate would be able to approach the zinc hydroxide from several sides of the cavity. The next event would be the addition of a protein-associated hydrogen bonding partner for the zinc hydroxide ion, represented by the hydroxyl group of Thr199 in the present day carbonic anhydrases. The function of this hydrogen-bond acceptor is to stabilize and provide the correct orientation of the zinc-bound hydroxide ion and to dictate the orientation of the bound bicarbonate. Consequently, the putative substrate binding sites are no longer equivalent; instead, the position closest to the deep-water Wat-338 becomes more efficient. Interestingly, the positioning of an obligate hydrogen-bond acceptor close to the free ligand position at the zinc ion seems to be essential in the carbonic anhydrase mechanism since it has evolved independently, by convergent evolution, in all three known classes (α, β, and γ) of carbonic anhydrases (*2*−*4*, *36*−*38*). The final step in the evolution of the enzyme would have included the creation of a hydrophobic pocket around the preferred site to increase the binding of the CO_2 molecule near a backbone amino group that facilitates the polarization and orientation of the CO_2 substrate.

ACKNOWLEDGMENT

We thank Katarina Wallgren for excellent technical assistance and Terese Bergfors for critical reading of the manuscript.

REFERENCES

1. Steiner, H., Jonsson, B. H., and Lindskog, S. (1975) *Eur. J. Biochem. 59*, 253−259.
2. Liljas, A., Kannan, K. K., Bergsten, P. C., Waara, I., Fridborg, K., Strandberg, B., Carlbom, U., Jarup, L., Lovgren, S., and Petef, M. (1972) *Nat. New. Biol. 235*, 131−137.
3. Eriksson, A. E., Jones, T. A., and Liljas, A. (1988) *Proteins 4*, 274−282.
4. Håkansson, K., Carlsson, M., Svensson, L. A., and Liljas, A. (1992) *J. Mol. Biol. 227*, 1192−1204.
5. Jonsson, B. H., Steiner, H., and Lindskog, S. (1976) *FEBS Lett. 64*, 310−314.
6. Simonsson, I., Jonsson, B. H., and Lindskog, S. (1979) *Eur. J. Biochem. 93*, 409−417.
7. Silverman, D. N., and Lindskog, S. (1988) *Acc. Chem. Res. 21*, 30−36.
8. Liang, Z., Xue, Y., Behravan, G., Jonsson, B. H., and Lindskog, S. (1993) *Eur. J. Biochem. 211*, 821−827.
9. Xue, Y., Liljas, A., Jonsson, B. H., and Lindskog, S. (1993) *Proteins 17*, 93−106.
10. Krebs, J. F., Ippolito, J. A., Christianson, D. W., and Fierke, C. A. (1993) *J. Biol. Chem. 268*, 27458−27466.
11. Lindskog, S., and Liljas, A. (1993) *Curr. Opin. Struct. Biol. 3*, 915−920.
12. Liljas, A., Hakansson, K., Jonsson, B. H., and Xue, Y. (1994) *Eur. J. Biochem. 219*, 1−10.
13. Xue, Y., Vidgren, J., Svensson, L. A., Liljas, A., Jonsson, B. H., and Lindskog, S. (1993) *Proteins 15*, 80−87.
14. Merz, K. M., Jr. (1990) *J. Mol. Biol. 214*, 799−802.
15. Kunkel, T. A. (1985) *Proc. Natl. Acad. Sci. U.S.A. 82*, 488−492.
16. Mårtensson, L. G., Jonasson, P., Freskgard, P. O., Svensson, M., Carlsson, U., and Jonsson, B. H. (1995) *Biochemistry 34*, 1011−1021.
17. Studier, F. W., and Moffatt, B. A. (1986) *J. Mol. Biol. 189*, 113−130.
18. Mårtensson, L. G., Jonsson, B. H., Andersson, M., Kihlgren, A., Bergenhem, N., and Carlsson, U. (1992) *Biochim. Biophys. Acta 1118*, 179−186.
19. Sanger, F., Nicklen, S., and Coulson, A. R. (1977) *Proc. Natl. Acad. Sci. U.S.A. 74*, 5463−5467.
20. Khalifah, R. G., Strader, D. J., Bryant, S. H., and Gibson, S. M. (1977) *Biochemistry 16*, 2241−2247.
21. Xue, Y., Jonsson, B. H., Liljas, A., and Lindskog, S. (1994) *FEBS Lett. 352*, 137−140.
22. Khalifah, R. G. (1971) *J. Biol. Chem. 246*, 2561−2573.
23. McPherson, A. (1982) *Preparation and Analysis of Protein Crystals*, pp 82−160, John Wiley and Sons, New York.
24. Otwinowski, Z., and Minor, W. (1997) *Methods Enzymol. 276*, 307−326.
25. Collaborative Computational Project Number 4. (1994) *Acta Crystallogr., Sect. D 50*, 760−763.
26. Brunger, A. T., Krukowski, A., and Erickson, J. W. (1990) *Acta Crystallogr., Sect. A 46*, 585−593.
27. Brunger, A. T. (1992) *Nature 355*, 472−474.
28. Jones, T. A., Zou, J. Y., Cowan, S. W., and Kjeldgaard. (1991) *Acta Crystallogr., Sect. A 47*, 110−109.
29. Murshudov, G. N., Vagin, A. A., and Dodson, E. J. (1997) *Acta Crystallogr., Sect. D 53*, 240−255.
30. Nair, S. K., and Christianson, D. W. (1991) *J. Am. Chem. Soc. 113*, 9455−9458.
31. Ippolito, J. A., Nair, S. K., Alexander, R. S., Kiefer, L. L., Fierke, C. A., and Christianson, D. W. (1995) *Protein Eng. 8*, 975−80.
32. Eriksson, A. E., Kylsten, P. M., Jones, T. A., and Liljas, A. (1988) *Proteins 4*, 283−293.
33. Tashian, R. E. (1989) *Bioessays 10*, 186−192.
34. Ippolito, J. A., Baird, T. T., Jr., McGee, S. A., Christianson, D. W., and Fierke, C. A. (1995) *Proc. Natl. Acad. Sci. U.S.A. 92*, 5017−5021.
35. Behravan, G., Jonsson, B. H., and Lindskog, S. (1990) *Eur. J. Biochem. 190*, 351−357.
36. Liljas, A., and Laurberg, M. (2000) *EMBO Rep. 1*, 16−7.
37. Kimber, M. S., and Pai, E. F. (2000) *Embo J. 19*, 1407−18.
38. Kisker, C., Schindelin, H., Alber, B. E., Ferry, J. G., and Rees, D. C. (1996) *Embo J. 15*, 2323−30.
39. Harris, M., and Jones, T. A. (2001) *Acta Crystallog., Sect. D 57*, 1201−1203.
40. Jackman, J. E., Merz, K. M., Jr., and Fierke, C. A. (1996) *Biochemistry 35*, 16421−16428.
41. Scolnick, L. R., and Christianson, D. W. (1996) *Biochemistry 35*, 16429−16434.
42. Nair, S. K., Calderone, T. L., Christianson, D. W., and Fierke, C. A. (1991) *J. Biol. Chem. 266*, 17320−17325.
43. Fierke, C. A., Calderone, T. L., and Krebs, J. F. (1991) *Biochemistry 30*, 11054−11063.
44. Alexander, R. S., Nair, S. K., and Christianson, D. W. (1991) *Biochemistry 30*, 11064−11072.
45. Krebs, J. F., Rana, F., Dluhy, R. A., and Fierke, C. A. (1993) *Biochemistry 32*, 4496−4505.
46. Nair, S. K., and Christianson, D. W. (1993) *Biochemistry 32*, 4506−4514.
47. Krebs, J. F., Fierke, C. A., Alexander, R. S., and Christianson, D. W. (1991) *Biochemistry 30*, 9153−9160.
48. Tweedy, N. B., Nair, S. K., Paterno, S. A., Fierke, C. A., and Christianson, D. W. (1993) *Biochemistry 32*, 10944−10949.
49. Ren, X. L., Jonsson, B. H., and Lindskog, S. (1991) *Eur. J. Biochem. 201*, 417−420.
50. Nair, S. K., Krebs, J. F., Christianson, D. W., and Fierke, C. A. (1995) *Biochemistry 34*, 3981−3989.
51. Kiefer, L. L., Krebs, J. F., Paterno, S. A., and Fierke, C. A. (1993) *Biochemistry 32*, 9896−9900.
52. Ippolito, J. A., and Christianson, D. W. (1993) *Biochemistry 32*, 9901−9905.

BI020053O